Appl Phys A (2011) 104:77–82
DOI 10.1007/s00339-011-6398-9

Applied Physics A
Materials Science & Processing

Influence of processing time on nanoparticle generation during picosecond-pulsed fundamental and second harmonic laser ablation of metals in tetrahydrofuran

Andreas Schwenke · Philipp Wagener · Stefan Nolte · Stephan Barcikowski

Received: 18 March 2011 / Accepted: 11 April 2011 / Published online: 11 May 2011

Abstract The influence of fundamental and second harmonic wavelength on ablation efficiency and nanoparticle properties is studied during picosecond laser ablation of silver, zinc, and magnesium in polymer-doped tetrahydrofuran. Laser ablation in stationary liquid involves simultaneously the fabrication of nanoparticles by ablation of the target material and fragmentation of dispersed nanoparticles by post irradiation. The ratio in which the laser pulse energy contributes to these processes depends on laser wavelength and colloidal properties. For plasmon absorbers (silver), using the second harmonic wavelength leads to a decrease of the nanoparticle productivity over process time along with exponential decrease in particle diameter, while using the fundamental wavelength results in a constant ablation rate and linear decrease in particle diameter. For colloids made of materials without plasmon absorption (zinc, magnesium), laser scattering is the colloidal property that limits nanoparticle productivity by Mie-scattering of dispersed nanoparticle clusters.

A. Schwenke · P. Wagener · S. Barcikowski (✉)
Laser Zentrum Hannover e.V., Hollerithallee 8, 30419 Hannover, Germany
e-mail: stephan.barcikowski@uni-due.de
Fax: +49-(0)201-1833049

S. Nolte
Institute of Applied Physics, Friedrich-Schiller-University Jena, Albert-Einstein-Straße 15, 07745 Jena, Germany

S. Barcikowski
Technical Chemistry I, University of Duisburg-Essen, Universitaetsstraße 5-7, 45141 Essen, Germany

1 Introduction

In recent years, intensive research has been done on the development of novel methods for the generation of nanoparticle colloids [1–4]. Pulsed laser ablation in liquids (PLAL) attracts more and more attention, since it can be used to generate colloids with outstanding purity, compared to conventional manufacturing methods [5]. This technique [6, 7] has been used to generate colloids based on metals [8, 9], alloys [10, 11], ceramics [12], and semiconductors [13] without impurities caused by chemical precursors or preservatives [5] in various liquids. Due to the fact that nanoparticles generated by PLAL are charged, it is possible to functionalize the nanoparticle surface in situ by doping the liquid before laser ablation with surfactants, ligands, monomers, or dissolved polymers, resulting in enhanced colloidal stability and matrix-coupling for polymer nanocomposites [14–16].

PLAL is mainly determined by (i) post irradiation, (ii) pulse duration, and (iii) laser wavelength.

(i) PLAL mainly employs processes in a stirred liquid [12] or with liquid recirculation [17], which results in a permanent change of process parameters due to increasing particle concentration and shielding of incoming laser beam. Therefore, PLAL includes at least two different processes: generation of nanoparticles by ablation of the target material and fragmentation of dispersed nanoparticles by post irradiation. The size of the nanoparticles after post irradiation mainly depends on laser parameters and on the presence of chemically active species like surfactants or capping agents in the solution [18]. The probability of particle fragmentation due to post irradiation is higher for shorter pulse durations. While particle fragmentation of colloids using nanosecond laser pulses is only possible at laser wavelengths with a sufficient absorption by the colloid, ul-

trashort laser pulses can reduce the particle size in colloids even with multiphoton absorption or white light continuum [18].

(ii) Pulse duration is also an important parameter for the generation of nanoparticles. By changing the pulse duration from nanoseconds (ns) to picoseconds (ps) toward femtoseconds (fs), the ablation mechanism changes from melting and thermal evaporation to phase explosion [19, 20]. The shorter the pulse duration, the more efficient the ablation process, including a nearly instantaneous evaporation with a minimized heat affected zone [21]. Lorazo et al. estimated a lower pulse duration limit of about 10 picoseconds for phase explosion [22]. Furthermore, it has been reported that primary plasma shielding is negligible for ultrashort laser pulses, as compared to nanosecond pulses [23, 24]. Consequently, using ultrashort laser pulse durations of picoseconds or femtoseconds has many advantages that can be used to enhance the efficiency of laser ablation process due to the absence of primary plasma shielding. The use of high-power picosecond pulses was successfully demonstrated by Bärsch et al. for the ablation of various materials in liquids [25].

(iii) Several research groups have found that for nanosecond pulses the yield of nanoparticles was significantly higher for ablation using the fundamental wavelength ($\lambda = 1064$ nm) than for second or third harmonic wavelength ($\lambda = 532$ nm or 355 nm) [26–28]. Procházka et al. demonstrated that an increasing number of irradiating nanosecond laser pulses using a laser wavelength of 1064 nm results in a decrease of the particle size in silver colloids [8]. They explained this effect by the absorption of the laser energy by colloidal particles. Mafuné et al. obtained a similar result for the irradiation of gold colloids using nanosecond pulses at 532 nm [29].

Reviewing of published papers in the area of nanoparticles generation using PLAL, Barcikowski et al. depict that most research examined either the generation of nanoparticles, or the fragmentation of dispersed nanoparticles [7]. As shown by Procházka et al. these processes cannot be studied separately in stationary liquid [8]. In this context, we compare the influence of fundamental and second harmonic laser wavelength on the ablation process and nanoparticle properties over process time during pulsed laser ablation of various metals in tetrahydrofuran using a high-power (50 W) picosecond-pulsed laser system. For the experimental objectives, which are high productivity and high particle concentration, we decided to compare both laser wavelengths at the highest possible pulse energy instead of the same pulse energy or the same laser fluence. Silver was chosen as a target material, due to its surface plasmon resonance in the range of the investigated laser wavelengths, and zinc and magnesium as representative base metals. Thermoplastic polyurethane (TPU)-doped tetrahydrofuran (THF) was chosen as liquid, because the generation of nanoparticles in an organic solution doped with dissolved polymer enables the transfer of generated nanoparticles into the polymer matrix simply by solvent casting. Furthermore, working in polymer-doped solvents is a straight-forward approach to integrate well-dispersed nanoparticles into a polymer matrix with a strong particle-matrix coupling [30].

2 Experimental details

The nanoparticle generation process using pulsed laser ablation in liquid is described in detail elsewhere [31]. In brief, laser ablation was carried out in a self-constructed ablation chamber at room temperature and atmospheric pressure in a polymer-doped tetrahydrofuran solution, using a high power picosecond laser system (Trumpf TruMicro 5050 and 5250) at the fundamental (1030 nm) and second harmonic (515 nm) laser wavelengths. The ablation chamber, made of Teflon, consists of a ring-shaped reservoir of about 30 ml in size, in which the fluid circulates with a constant volume flow provided by a motor driven stirrer. The optical path length between the entrance window, made of antireflective coated quartz glass, and the metal target is 6 mm.

The picosecond laser system provides pulses of 7 ps duration with a maximum pulse energy of 250 µJ at the fundamental laser wavelength (1030 nm), or a maximum of 125 µJ at the second harmonic laser wavelength (515 nm). Experiments have been carried out at a repetition rate of 33 kHz. The irradiation was guided by a laser scanner (Scanlab, HurryScan II-14) with a fixed spiral scan pattern (diameter 5 mm, interline distance 50 µm) and an applied scan speed of 3.3 m/s, resulting in a spatial interpulse distance of 100 µm. The laser beam was focused through a telecentric F-theta lens (Sill Optics) with a focal length of 56 mm. To position the ablation chamber along the beam axis, the chamber was attached on a manually controlled micrometer XY stage. The amount of ablated mass was determined by differential weighing of the target using microbalances (Sartorius M3P, accuracy ±0.001 mg; Sartorius R160P, accuracy ±0.01 mg). The targets were irradiated for different ablation times up to 60 minutes. Tetrahydrofuran (Sigma-Aldrich, >99.9%) was doped with 0.3% dissolved thermoplastic polyurethane (Elastollan 1190 A; BASF Polyurethanes) to enhance the stability of the colloids, according to earlier results [16]. Targets made of silver, magnesium, and zinc (each 10×10 mm^2) were prepared from a 1 mm thick foil (Good Fellow, >99.95% purity). To determine laser fluence, spot diameters were measured using light microscopy. Analyses of hydrodynamic particle size in solution were done using dynamic light scattering (Malvern

Zetasizer). The optical absorption spectra of the resulting colloids were measured using UV–VIS spectroscopy (Shimadzu 1650). STEM analyses were made on thin films, which arose on carbon-coated Formvar copper grids after dipping in colloids. Primary particle size (Feret diameter) was measured for at least 200 particles.

3 Results and discussion

In Fig. 1, the cumulative ablated mass of silver (Fig. 1a), magnesium (Fig. 1b), and zinc (Fig. 1c) is displayed over the process interval, from one minute up to 60 minutes for ablation using fundamental and second harmonic laser wavelengths. For comparison of the maximal possible productivity, which means the amount of nanoparticles over time, both laser systems were operated at their highest possible pulse energy as described above. For all three investigated materials, picosecond laser ablation in TPU-doped tetrahydrofuran using the fundamental wavelength yields a much higher ablated mass after the same process time than with the second harmonic wavelength. While it is obvious that the fundamental laser wavelength provides pulse energy twice as high as the second harmonic laser wavelength (250 µJ for 1030 nm compared to 125 µJ for 515 nm), the most important parameter for pulsed laser ablation in liquid is the resulting laser fluence on the target surface. On the basis of linear optics, the resulting laser spot diameter should be half the size for the second harmonic, compared with the fundamental laser wavelength, resulting in doubled laser fluence, although using half the pulse energy. However, when ultrashort laser pulses pass through the liquid, nonlinear effects occur, which lead to a filamentation of the laser beam. The threshold of filamentation for picosecond pulses in THF is in the order of 1.6 MW, which is significantly lower than in our experimental setting. Therefore, the difference in the measured spot diameter (fundamental: 300 nm; second harmonic: 270 nm; analyzed with light microscope) does not equal expectations based on linear optics, resulting in a laser fluence of approximately 0.35 J/cm^2 for fundamental, and 0.22 J/cm^2 for second harmonic wavelengths. In conclusion, higher pulse energy and subsequent higher laser fluence for the fundamental laser wavelength results in higher nanoparticle generation productivity.

During ablation of silver in THF/TPU, there is a strong correlation between the absorption of the colloid at the laser wavelength used, and the ablation rate as well as the resulting hydrodynamic particle size (Figs. 1a and 2). The cumu-

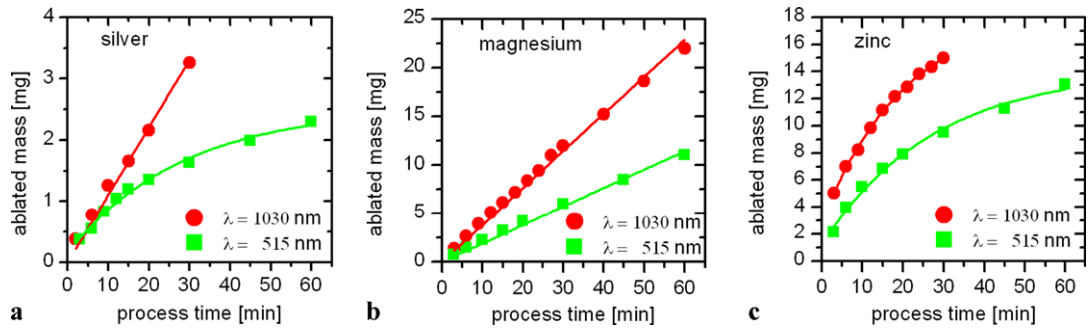

Fig. 1 Effect of wavelength and material on nanoparticle productivity; cumulative ablated mass over processing time of silver (**a**), magnesium (**b**) and zinc (**c**) for ablation in THF using fundamental (1030 nm; 250 µJ) and second harmonic (515 nm; 125 µJ) laser wavelengths

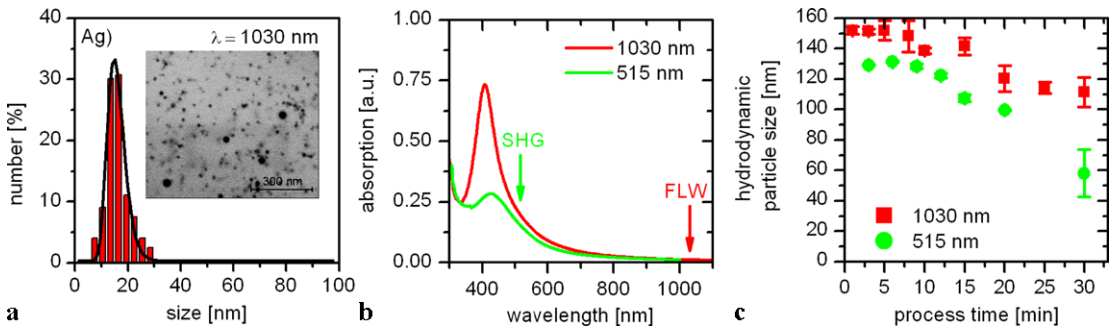

Fig. 2 Properties of colloids after laser ablation of silver in polyurethane-doped THF; primary particle diameter and STEM analysis of Ag–TPU nanocomposites made using the fundamental laser wavelength (**a**), optical spectra of Ag–THF/TPU colloids generated using the fundamental and second harmonic wavelength after 30 minutes (**b**), changes in hydrodynamic particle diameter of Ag–THF/TPU colloids over process time for ablation using fundamental and second harmonic laser wavelengths (**c**)

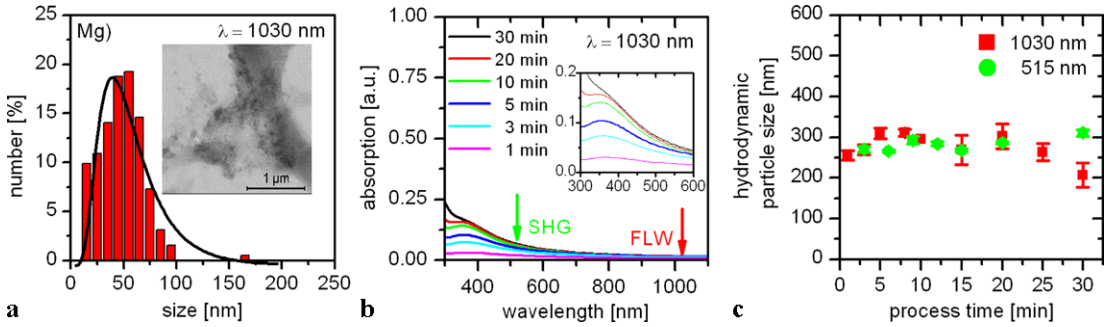

Fig. 3 Properties of colloids after laser ablation of magnesium in polyurethane-doped THF; primary particle diameter and STEM analysis of MgO–TPU nanocomposites made using the fundamental laser wavelength (**a**), optical spectra of MgO–THF/TPU colloids generated using the fundamental wavelength for different process times (**b**), hydrodynamic particle diameter of MgO–THF/TPU colloids over process time for ablation using the fundamental and second harmonic laser wavelengths (**c**)

lative ablated mass increases linearly for ablation using the fundamental laser wavelength, while saturation occurs for ablation using the second harmonic wavelength (Fig. 1a). After 30 minutes, the cumulative ablated mass for ablation using the red wavelength (3.3 mg) is twice as high as for ablation using the green wavelength (1.6 mg). Representative primary particle diameter distribution resulting from laser ablation of silver using the fundamental laser wavelength is shown in Fig. 2a. STEM images of Ag–TPU nanocomposites indicate a primary particle size of approximately 15 nm (log-normal fit, peak maximum) with well-dispersed nanoparticles embedded into the polymeric matrix of thermoplastic polyurethane. Absorption spectra of Ag–THF/TPU colloids prepared using ablation with second harmonic and fundamental laser wavelengths after a process interval of 30 minutes (Fig. 2b) consist of a strong absorption peak, due to surface plasmon resonance (SPR) around 400 nm. The peak intensity of the silver colloid produced using the fundamental laser wavelength is much higher compared to the colloid produced using the second harmonic wavelength, due to the higher particle concentration (see Fig. 1a). While the analysis of the primary particle size is suitable for the characterization of nanoparticle properties in a solid nanocomposite, properties in colloids are described by the analysis of the hydrodynamic particle diameter measured with dynamic light scattering. The hydrodynamic particle diameter equals the diameter of a sphere describing the movement of a nanoparticle in THF with polymer coating and solvation shell including clustering of several particles. Changes of hydrodynamic particle diameter in Ag–THF/TPU colloids during ablation using red and green laser wavelengths are presented in Fig. 2c. Differences in the hydrodynamic particle size (115 nm) and the primary particle size (15 nm) are caused by the solvation shell and TPU shell around the nanoparticles in the colloid. While there is an almost linear decrease in hydrodynamic particle size during fundamental laser ablation from 150 nm to 115 nm, the hydrodynamic particle diameter decreases exponentially for second harmonic laser ablation from 130 nm to 60 nm. Loss of excitation light by absorption or scattering of the silver colloid is weak at the fundamental laser wavelength of 1030 nm, and increases only very slightly over process time, resulting in a linear ablation rate and a slight, almost linear decrease in hydrodynamic particle size. Ablation using the second harmonic wavelength (515 nm) is strongly affected by losses of excitation light due to surface plasmonic resonance, resulting in saturation of cumulative ablated mass during process time. The increase in laser energy, absorbed by the colloid, results in an exponential decrease of the hydrodynamic particle size. The exponential decrease could be assigned to particle fragmentation during post irradiation of dispersed nanoparticles. Absorption of laser energy is the most important impulse for particle fragmentation. This decrease is in good correlation with results of Procházka et al. [8] and Mafune [29] for irradiation with nanosecond pulses.

As expected, the conditions for the ablation of magnesium are different compared to silver. For both laser wavelengths, there is a linear increase of the total ablated mass with different slopes without a change in hydrodynamic particle size (Figs. 1b and 3c). As shown in Fig. 3b, even after 30 minutes of ablation, only a weak absorption occurs for fundamental wavelengths, and a slightly higher absorption for second harmonic wavelengths. Both absorption rates are not sufficient to lower the ablation rate over the investigated process interval of up to 60 minutes. Furthermore, the absorbed laser energy does not reach sufficient values for particle fragmentation by post irradiation, resulting in an unchanged hydrodynamic particle diameter over the investigated process time. Therefore, ablation using fundamental and second harmonic laser wavelengths is not effected by high losses of excitation light, resulting in constant ablation rates for both wavelengths. Representative primary particle diameter distribution resulting from

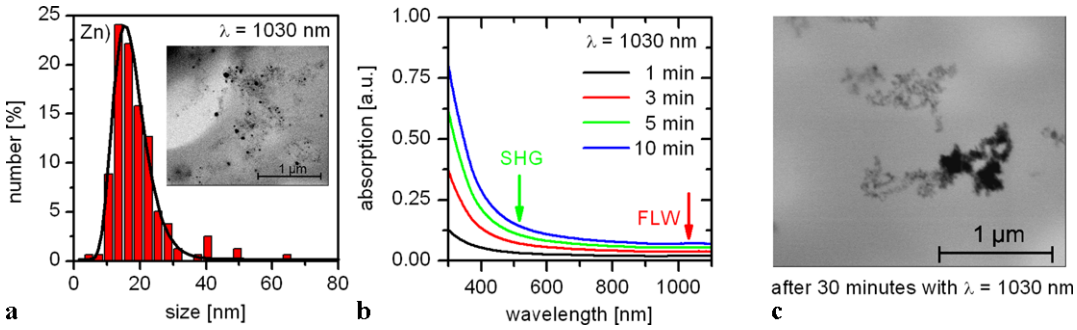

Fig. 4 Properties of colloids after laser ablation of zinc in polyurethane-doped THF; primary particle diameter and STEM analysis of ZnO–TPU nanocomposites made using the fundamental laser wavelength (**a**), optical spectra of ZnO–THF/TPU colloids generated using the fundamental laser wavelength for different process times (**b**), STEM analysis of agglomerated ZnO–TPU nanocomposites generated using the fundamental laser wavelength after a process time of 30 minutes (**c**)

laser ablation of magnesium using fundamental laser wavelength indicates a mean primary particle diameter of approximately 51 nm with a broad particle size distribution (Fig. 3a). Due to the weak contrast between Mg nanoparticles and the TPU matrix in STEM analyses, determination of the primary nanoparticle size for magnesium is not as precise as for silver. As mentioned for silver, the difference in hydrodynamic (280 nm) and primary particle size (51 nm) is caused by the TPU shell and agglomeration. Due to the fact that magnesium is a base metal with the tendency to oxidize in an atmosphere with sufficient oxygen content, it is most likely that for the ablation of magnesium in THF/TPU, resulting nanoparticles consist of MgO. Only few research results can be found for the generation of Mg/MgO nanoparticles using PLAL. Phuoc et al. investigated nanosecond-pulsed laser ablation of magnesium in SDS solutions and acetone. Laser ablation in aqueous SDS solutions yielded brucite $Mg(OH)_2$ nanoparticles with different crystallinity and morphology, depending on the specific SDS concentrations [32]. Resulting colloids only exhibited characteristics of Rayleigh scattering without peak absorption. The UV–VIS spectrum of colloids prepared in acetone exhibited characteristic absorption bands with a single absorption peak located near 330 nm [32]. Corresponding XRD patterns indicate a coexistence of Mg and MgO [32]. Regarding our experiments, UV–VIS spectra of ablated magnesium in THF/TPU using the fundamental laser wavelength exhibit an absorption peak at 350 nm (Fig. 3b). The difference in peak position (Mg/MgO in THF/TPU: 350 nm; Mg/MgO in acetone: 330 nm) can be explained by bathochromic peak shifting due to the TPU shell and different solvent.

Similar to magnesium, zinc is a base metal with the tendency to oxidize, and without plasmon resonance at investigated laser wavelengths. For both laser wavelengths, saturation occurs with a lower saturation value for the second harmonic wavelength (Fig. 1c). The mean primary particle diameter of resulting nanoparticles is 17 nm for ablation using the fundamental wavelength (Fig. 4a). The absorption spectra of colloids prepared by ablation using the infrared wavelength for different process times up to 10 minutes consist of a nonlinear strong absorption rise in the UV range, super positioned with a continuously growing wavelength independent off-set (Fig. 4b). With increasing process time, nanoparticles tend to agglomerate, and precipitation occurs, which made measurement of optical spectra dispensable. STEM analysis of the agglomerated nanoparticles after a process time of 30 minutes with a secondary particle size of about 1 µm is shown in Fig. 4c. Earlier investigations proved that for the ablation of zinc in THF/TPU, the nanoparticles are composed of zinc oxide covered by a TPU shell [30]. Nevertheless, we could not find an absorption band for zinc oxide at 350 nm. As the absorption in UV can be explained by Rayleigh scattering of particles smaller than the laser wavelength, the continuously growing wavelength independent off-set corresponds to Mie scattering for larger agglomerated nanoparticles. Within the range of investigated materials, colloidal stability is the weakest for the ablation of zinc in THF/TPU, resulting in agglomeration and precipitation during the process (Fig. 4c). Scattering for these microparticles, consisting of agglomerated nanoparticles, is almost independent of the wavelength, so a similar ablation behavior could be found for fundamental and second harmonic wavelengths. In conclusion, ablation using the fundamental wavelength is not affected by Rayleigh scattering but by Mie scattering, resulting in a slow saturation of the nanoparticle mass productivity for zinc. Ablation using the second harmonic wavelength is affected by Rayleigh scattering and Mie scattering, resulting in faster productivity saturation, compared to ablation using the fundamental laser wavelength. For the investigated metals, zinc is the only material with saturation in cumulative ablated mass at the fundamental laser wavelength, which can be explained on the basis of absorption spectra consisting of a distinctive scattering in the range of near infrared.

4 Conclusions

In conclusion, picosecond-pulsed laser ablation in a stationary liquid is mainly affected by two processes: the generation of nanoparticles, due to laser energy absorbed by the target, and the fragmentation of dispersed nanoparticles by post irradiation due to laser energy absorbed by the colloidal nanoparticles. Picosecond laser ablation of Ag, Zn, or Mg in polyurethane-doped tetrahydrofuran using the fundamental wavelength (1030 nm) yields a much higher ablated mass after the same process time than for the second harmonic wavelength of 515 nm, which can be explained due to the higher pulse energy (250 μJ for fundamental and 125 μJ for second harmonic) and subsequent higher laser fluence (0.35 J/cm^2 and 0.22 J/cm^2, respectively). For silver, as an exemplary material for colloids with strong absorption due to surface plasmon resonance in the range of the second harmonic laser wavelength, ablation efficiency decreases over process time, while it is constant for the fundamental laser wavelength. For both wavelengths, particle fragmentation during post irradiation occurs, which is stronger for the second harmonic wavelength, due to higher absorption. As MgO–THF/TPU and ZnO–THF/TPU colloids have no absorption peak at the investigated laser wavelengths, scattering of laser energy is the determining colloidal property for ablation rate. For MgO–THF/TPU, only weak scattering in terms of Rayleigh scattering occurred, resulting in linear ablation rates for both laser wavelengths. For ZnO–THF/TPU, due to precipitation and agglomeration, high Mie scattering results in saturation of cumulative ablated mass for both laser wavelengths.

In conclusion, to choose the appropriate laser wavelength for picosecond laser ablation in liquids, different aspects have to be balanced. For high productivity of concentrated nanoparticle colloids, fundamental wavelength is always more suitable than second harmonic wavelength. If particle size reduction by fragmentation of plasmon resonant nanoparticles is desired, second harmonic laser wavelength is more effective than fundamental laser wavelength. Furthermore, laser ablation in tetrahydrofuran is a straightforward approach to integrate nanoparticles into a polymer matrix.

Acknowledgements The work was supported by the German Federal Ministry of Education and Research (BMBF) within the project NanoKOMED (FKZ 13N9799) and by the German Research Foundation (DFG) within the priority program SPP 1327.

References

1. M. Brust, M. Walker, D. Bethell, D.J. Schiffrin, R. Whyman, J. Chem. Soc., Chem. Commun. **801** (1994)
2. Y. Sun, B. Whiley, Z.Y. Li, Y. Xia, J. Am. Chem. Soc. **126**, 9399 (2004)
3. R.N. Grass, W.J. Stark, J. Mater. Chem. **16**, 1825 (2006)
4. T. Tsuji, T. Hamagami, T. Kawamura, J. Yamaki, M. Tsuji, Appl. Surf. Sci. **243**, 214 (2005)
5. J.A. Dahl, B.L.S. Maddux, J.E. Hutchison, Chem. Rev. **107**, 2228 (2007)
6. V. Amendola, M. Meneghetti, Phys. Chem. Chem. Phys. **11**, 3805–3821 (2009)
7. S. Barcikowski, F. Devesa, K. Moldenhauer, J. Nanopart. Res. **11**, 1883–1893 (2009)
8. M. Procházka, P. Mojzeš, J. Štepánek, B. Vlèková, P.-Y. Turpin, Anal. Chem. **69**, 5103 (1997)
9. F. Mafuné, J. Kohno, Y. Takeda, T. Kondow, H. Sawabe, J. Phys. Chem. B **104**, 8333 (2000)
10. A.V. Kabashin, M. Meunier, J. Appl. Phys. **94**, 7941 (2003)
11. A.V. Simakin, V.V. Voronov, N.A. Kirichenko, G.A. Shafeev, Appl. Phys. A, Mater. Sci. Process. **79**, 1127 (2004)
12. N. Bärsch, A. Gatti, R. Sattari, S. Barcikowski, J. Laser Micro Nanoeng. **4**, 66 (2009)
13. H. Zeng, W. Cai, Y. Li, J. Hu, P. Liu, J. Phys. Chem. B **109**, 18260 (2005)
14. S. Besner, A.V. Kabashin, F.M. Winnik, M. Meunier, J. Phys. Chem. C **113**, 9526 (2009)
15. T. Tsuji, D.-H. Thang, Y. Okazaki, M. Nakanishi, Y. Tsuboi, M. Tsuji, Appl. Surf. Sci. **254**, 5224 (2008)
16. P. Wagener, G. Brandes, A. Schwenke, S. Barcikowski, Phys. Chem. Chem. Phys. **13**, 5120 (2011)
17. S. Barcikowski, A. Menéndez-Manjón, B.N. Chichkov, M. Brikas, G. Raèiukaitis, Appl. Phys. Lett. **91**, 083113 (2007)
18. S. Besner, A.V. Kabashin, M. Meunier, Appl. Phys. Lett. **89**, 233122 (2006)
19. S. Nolte, C. Momma, H. Jacobs, A. Tünnermann, B.N. Chichkov, B. Wellegehausen, H. Welling, J. Opt. Soc. Am. B **14**, 2716 (1997)
20. R. Kelly, A. Miotello, Appl. Surf. Sci. **205**, 96 (1996)
21. C. Momma, B.N. Chichkov, S. Nolte, F. Von Alvensleben, A. Tünnermann, H. Welling, B. Wellegehausen, Opt. Commun. **129**, 134 (1996)
22. P. Lorazo, L.J. Lewis, M. Meunier, Phys. Rev. Lett. **91**, 225501 (2003)
23. K. Patahk, A. Povitsky, J. Appl. Phys. **104**, 113108 (2008)
24. A. Ancona, F. Röser, K. Rademaker, J. Limpert, S. Nolte, A. Tünnermann, Opt. Express **16**, 8958 (2008)
25. N. Bärsch, J. Jakobi, S. Weiler, S. Barcikowski, Nanotechnology **20**, 44 (2009)
26. T. Tsuji, K. Iryo, N. Watanabe, M. Tsuji, Appl. Surf. Sci. **202**, 80 (2002)
27. P. Šmejkal, J. Pfleger, B. Vlčková, O. Dammer, J. Phys. Conf. Ser. **59**, 185 (2007)
28. W.T. Nichols, T. Sasaki, N. Koshizaki, J. Appl. Phys. **100**, 114912 (2006)
29. F. Mafuné, J. Kohno, Y. Takeda, T. Kondow, H. Sawabe, J. Phys. Chem. B **105**, 5114 (2001)
30. P. Wagener, S. Faramarzi, A. Schwenke, R. Rosenfeld, S. Barcikowski, Appl. Surf. Sci. **257**, 7231 (2011)
31. P. Wagener, A. Schwenke, B.N. Chichkov, S. Barcikowski, J. Phys. Chem. C **114**, 7618 (2010)
32. T.X. Phuoc, B.H. Howard, D.V. Martello, Y. Soong, M.K. Chyu, Opt. Lasers Eng. **46**, 829 (2008)